Article

Three New Lanthanum Oxoantimonate(III) Halides: Synthesis and Crystal Structure of La$_5$Cl$_3$[SbO$_3$]$_4$, La$_2$Sb$_{12}$O$_{19}$Br$_4$ and La$_2$Sb$_{12}$O$_{19}$I$_4$

Ralf J. C. Locke [1], Kim-Natalie Bozenhardt [1], Felix C. Goerigk [1,2] and Thomas Schleid [1,*]

[1] Institute for Inorganic Chemistry, University of Stuttgart, D-70569 Stuttgart, Germany
[2] Leuchtstoffwerk Breitungen GmbH, D-98597 Breitungen, Germany
* Correspondence: schleid@iac.uni-stuttgart.de

Abstract: It was possible to synthesize colorless single crystals of La$_5$Cl$_3$[SbO$_3$]$_4$ (block-shaped) as well as La$_2$Sb$_{12}$O$_{19}$Br$_4$ and LaSb$_{12}$O$_{19}$I$_4$ (both needle-shaped), representing three new compounds from the system of lanthanum oxoantimonate(III) halides, which have not been described in the literature before. La$_5$Cl$_3$[SbO$_3$]$_4$ crystallizes in the monoclinic space group $P2/c$ with the lattice parameters $a = 895.82(5)$ pm, $b = 564.28(3)$ pm, $c = 1728.19(9)$ pm, and $\beta = 90.007(2)°$ for $Z = 2$. This layered compound contains isolated ψ^1-tetrahedral [SbO$_3$]$^{3-}$ units, square hemiprisms [LaO$_8$]$^{13-}$, and antiprisms [LaO$_4$Cl$_4$]$^{9-}$. La$_2$Sb$_{12}$O$_{19}$Br$_4$ and LaSb$_{12}$O$_{19}$I$_4$ crystallize isotypically in the orthorhombic space group $Pnma$ with $a = 3184.69(19)$ pm, $b = 417.78(3)$ pm, $c = 1019.85(6)$ pm for the bromide and $a = 3215.08(19)$ pm, $b = 419.94(3)$ pm, $c = 1062.89(6)$ pm for the iodide. Instead of isolated [SbO$_3$]$^{3-}$ anions, semi-tubular features $^1_\infty\{$[Sb$_{12}$O$_{19}$]$^{2-}\}$ are present, which consist mainly of [SbO$_4$]$^{5-}$ and few [SbO$_3$]$^{3-}$ units with stereochemically active electronic lone pairs at their Sb^{3+} centers. Within these so-called "double-halfpipes", La^{3+} is surrounded by nine oxygen atoms as [LaO$_9$]$^{15-}$ polyhedron without any contact with X^- anions. Single-crystal Raman measurements were performed for La$_5$Cl$_3$[SbO$_3$]$_4$ and LaSb$_{12}$O$_{19}$I$_4$, and La$_5$Cl$_3$[SbO$_3$]$_4$ was structurally compared with the isostoichiometric, but not isotypic La$_5$F$_3$[SbO$_3$]$_4$.

Keywords: lanthanum; oxoantimonates(III); halides; crystal structures; Raman spectra

1. Introduction

Because different structures for compounds with the general composition RE_5X_3[AsO$_3$]$_4$ (RE = Y, La–Nd, Sm–Lu; X = F–Br) have already been described from several previous investigations into the quaternary systems RE–X–As–O, interest has now switched to exploring this composition type by moving from arsenic to antimony as the heavier homolog. The aim was to uncover possibly existing structural similarities or differences between these halide derivatives of oxoarsenates(III) and -antimonates(III). While the fluoride derivatives with the composition RE_5F$_3$[AsO$_3$]$_4$ (RE = Y, Ho, Tm–Lu) [1–3] exhibit a tetragonal crystal structure (space group: $P4/ncc$), the analogous chlorides (RE_5Cl$_3$[AsO$_3$]$_4$ with RE = La–Nd and Sm) [2,4,5] and bromides (RE_5Br$_3$[AsO$_3$]$_4$ with RE = Pr, Sm, Eu, and Tb) [2,3,6] occur with different monoclinic crystal structures in the space groups $P2/c$ or $C2/c$. For the corresponding oxoantimonates(III) with the composition RE_5X_3[SbO$_3$]$_4$, only the lanthanum representative La$_5$F$_3$[SbO$_3$] [7] has been known in literature since 1988 and shows the same crystal structure as the fluoride oxoarsenates(III) RE_5F$_3$[AsO$_3$]$_4$ [1–3]. Other antimonates(III) of this composition have not yet been described in the literature. The influence of both the lone-pair of electrons at the Pn^{3+} centers (Pn = As and Sb) of the involved [PnO$_3$]$^{3-}$ anions and the differently hard X^- anions (X = F–I) on potential luminescence properties of the RE^{3+} cations have triggered our activities for further investigations. Moreover, the existence of completely different compositions and crystal structures for the tetragonal oxobismuthate(III) halides REBi$_2$O$_4X$ (RE = Y, La, Pr, Nd, Sm–Lu, X = Cl–I) [6,8–11], crystallizing in space group $P4/mmm$, was encouragement

enough for more systematic studies. First results on the oxoantimonate(III)-halide branch have revealed that the tetragonal RESb$_2$O$_4$Cl representatives for RE = Sm and Eu [6,12] crystallize in space group $P4/ncc$, but for RE = Y, Gd–Lu [3,6,13,14] in space group $P42_12$, whereas the RESb$_2$O$_4$Br representatives with RE = Y, Eu–Dy [3,6,13,15,16] prefer the monoclinic space group $P2_1/c$. All before-mentioned investigations have so far shown that for As^{3+} exclusively isolated [AsO$_3$]$^{3-}$ anions are present as ψ^1-tetrahedral trigonal pyramids, while for the Sb^{3+} case the analogous units [SbO$_3$]$^{3-}$ aspire to an extra oxygen contact for their central Pn^{3+} cation, which becomes a general feature in the oxobismuthate(III) halides, where vertex-sharing [BiO$_4$]$^{5-}$ units dominate as ψ^1_{ax}-square pyramids for the heaviest Pn^{3+} congener. The influence of the halide anions X^- (X = F–I) on the actual crystal structures seems to be intriguing as well, so we started our corresponding research with the system La–X–Sb–O.

2. Materials and Methods

2.1. Product Synthesis

According to the literature, for the synthesis of La$_5$F$_3$[SbO$_3$]$_4$, the preparation of La$_5$Cl$_3$[SbO$_3$]$_4$ was carried out according to Equation (1) with the reactants lanthanum sesquioxide (La$_2$O$_3$ (656 mg, 0.336 mmol): ChemPur, 99.99%), lanthanum trichloride (LaCl$_3$ (246 mg, 0.336 mmol): ChemPur, 99.9%), antimony sesquioxide (Sb$_2$O$_3$ (583 mg, 0.168 mmol): ChemPur, 99.9%) and as flux cesium chloride (CsCl (800 mg): Aldrich, 99.9%) at a temperature of 780 °C for a period of four days, followed by slow cooling to 660 °C and further keeping this temperature for four more days, and subsequent cooling to room temperature. Thereafter, the aqueous workup to remove the flux yielded a fibrous microcrystalline powder containing a few octahedrally shaped single crystals (Figure 1), which had the desired composition and could be further characterized by single-crystal X-ray diffraction.

$$2\,La_2O_3 + LaX_3 + 2\,Sb_2O_3 \rightarrow La_5X_3[SbO_3]_4 \text{ (Flux: CsX, X = Cl)} \tag{1}$$

Figure 1. Electron micrograph of some crystals with the composition La$_5$Cl$_3$[SbO$_3$]$_4$. The long rods visible at the upper edge of the image originate from a silicate by-product (apatite-type La$_{4.667}$O[SiO$_4$]$_3$ [17]).

In synthesis experiments of $LaSb_2O_4Br$ and $LaSb_2O_4I$ according to reaction Equation (2), lanthanum sesquioxide (La_2O_3 (52 mg, 0.158 mmol or 47 mg, 0.145 mmol): ChemPur, 99.99%) was reacted with the lanthanum trihalides ($LaBr_3$ (60 mg, 0.158 mmol): ChemPur, 99.9%; LaI_3 (76 mg, 0.145 mmol): ChemPur, 99.9%, respectively) and antimony sesquioxide (Sb_2O_3 (138 mg, 0.053 mmol or 127 mg, 0.048 mmol): ChemPur, 99.9%) to yield the new lanthanum oxoantimonate(III) halides $La_2Sb_{12}O_{19}X_4$ (X = Br or I). Cesium bromide (CsBr (800 mg): Aldrich, 99.9%) or cesium iodide (CsI (800 mg): Merck, 99.99%) were chosen as fluxes, and the reactions always took place in evacuated glassy silica ampoules. Their content reacted in a muffle furnace (Nabertherm, L9/12) at a specific temperature program. This involved heating to 750 °C at a rate of 150 °C/h and holding this temperature for two more days. Then, cooling with a rate of 5 °C/h brought the vials to 666 °C, and again, keeping this temperature for two days was useful. Renewed cooling at 5 °C/h took the ampoules down to 530 °C, whereafter this temperature was maintained for two more days. In the final step, cooling at 10 °C/h to 480 °C and finally at 150 °C/h to room temperature took place. The reaction products were then washed with demineralized water and dried at 120 °C in a drying oven. Needle-shaped single crystals (Figure 2) were easily found under a stereomicroscope.
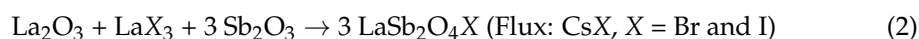
$$La_2O_3 + LaX_3 + 3\,Sb_2O_3 \rightarrow 3\,LaSb_2O_4X \text{ (Flux: Cs}X, X = \text{Br and I)} \tag{2}$$

Figure 2. Electron-microscopic backscattering image of some acicular crystals of composition $La_2Sb_{12}O_{19}Br_4$.

2.2. Single-Crystal X-ray Diffraction

Suitable crystals of all three lanthanum oxoantimonate(III) halides were selected from the samples and fixed in glass capillaries (Hilgenberg, Malsfeld; outer diameter: 0.1 mm, wall thickness: 0.001 mm) with grease. The measurements occurred with a four-circle single-crystal diffractometer κ-CCD (Bruker-Nonius, Karlsruhe, Germany) for $La_5Cl_3[SbO_3]_4$ and a single-crystal diffractometer STADI-VARI (Stoe, Darmstadt, Germany) for $La_2Sb_{12}O_{19}Br_4$ and $La_2Sb_{12}O_{19}I_4$. The monoclinic crystal structure of $La_5Cl_3[SbO_3]_4$ was solved using direct methods in the centrosymmetric space group $P2/c$ and refined using the SHELX-97 program package [18,19]. The orthorhombic crystal structures of $La_2Sb_{12}O_{19}Br_4$ and $La_2Sb_{12}O_{19}I_4$ were determined in the centrosymmetric space group *Pnma* with the same methods.

2.3. Raman Spectroscopy

Raman spectra of the single crystals of $La_5Cl_3[SbO_3]_4$ and $La_2Sb_{12}O_{19}I_4$ were recorded using a Raman microscope (XploRA, Horiba, Kyoto, Japan) with an excitation wavelength of λ = 638 nm ($La_5Cl_3[SbO_3]_4$) and λ = 532 nm ($La_2Sb_{12}O_{19}I_4$) at a LASER power of 25 mW.

2.4. Electron-Beam Microprobe Analysis

Scanning electron microscope (SEM) images of $La_5Cl_3[SbO_3]_4$ and $La_2Sb_{12}O_{19}Br_4$ were acquired using an electron-beam microprobe system (SX-100, Cameca, Gennevilliers, France).

2.5. Powder X-ray Diffraction

The sample of $La_5Cl_3[SbO_3]_4$ was measured in transmission geometry on a Rigaku SmartLab X-ray powder diffractometer (Rigaku, Tokyo, Japan) using Cu-$K_{\alpha 1}$ radiation. Figure 3 shows the powder diffractogram. It contains traces of CsCl and an unknown phase (marked with 2) in addition to $La_5Cl_3[SbO_3]_4$. Further reflections of elemental cubic aluminum (marked with 1) result from the measurement on an aluminum sample carrier.
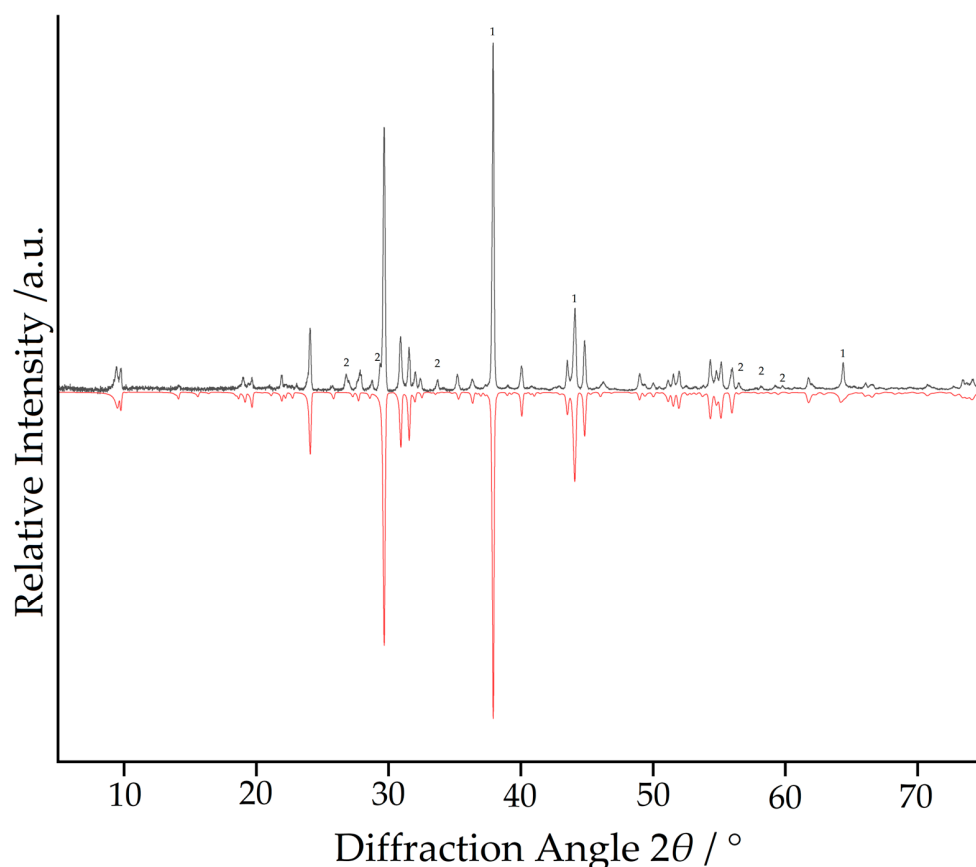

Figure 3. Powder X-ray diffractogram of $La_5Cl_3[SbO_3]_4$ (the reflections marked with 1 belong to cubic aluminum, and the ones marked with 2 originate from an unknown phase). In black the measurement and in red the theoretical data.

The analogously recorded powder X-ray diffractograms of $La_2Sb_{12}O_{19}Br_4$ and $La_2Sb_{12}O_{19}I_4$ are not shown, despite the fact that they also show the presence of the title compounds. Moreover, they document that these products do not occur in phase pure, which is already assumable by their formation reaction (Equation (2)), targeting the compositions $LaSb_2O_4Br$ and $LaSb_2O_4I$. In the first case, there is strong evidence for the presence of $La_5Br_3[SbO_3]_4$ as a by-product, which most probably crystallizes isotypically with $La_5Cl_3[SbO_3]_4$. The formation of this compound with a molar ratio of La:Sb = 5:4 would explain the dominance of the $La_2Sb_{12}O_{19}Br_4$

phase (La:Sb ratio = 1:6) when a compound such as $LaSb_2O_4Br$ (La:Sb ratio = 1:2) is planned to be synthesized. For the $La_2Sb_{12}O_{19}I_4$ case, there are many extra reflections in the powder X-ray diffractogram, which originate from a cesium-containing by-product with the composition $CsI_4La_2Sb_{8.333}O_{14}$ (monoclinic, $C2/m$; $a \approx 2325$ pm, $b \approx 420$ pm, $c \approx 1300$ pm, $\beta \approx 96.5°$ for $Z = 2$) crystallizing isotypically with $RbI_4Nd_2Sb_{8.333}O_{14}$ [20,21] after the incorporation of some CsI from the flux (Equation (2)). As the empirical formula $Cs_2I_8La_4Sb_{16.667}O_{28}$ for $Z = 1$ already suggests, there are strong structural similarities to $La_2Sb_{12}O_{19}I_4$, which will be shown in an upcoming publication soon.

3. Results and Discussion

3.1. Crystal Structures of $La_5Cl_3[SbO_3]_4$ and $La_5F_3[SbO_3]_4$ in Comparison

$La_5Cl_3[SbO_3]_4$ crystallizes monoclinically in the space group $P2/c$ with the lattice parameters $a = 895.82(5)$ pm, $b = 564.28(3)$ pm, $c = 1728.19(9)$ pm and $\beta = 90.007(2)°$ for two formula units per unit cell. Three distinct crystallographic positions result for the La^{3+} cations, each having a coordination number of *C.N.* = 8, but the coordinating particles differ to some extent. $(La1)^{3+}$ and $(La2)^{3+}$ are surrounded eightfold by oxygen atoms in the form of square antiprisms or hemiprisms $[LaO_8]^{13-}$ with lanthanum-oxygen distances in the range of d(La1–O) = 237–264 pm and d(La2–O) = 230–262 pm (Figure 4, *left* and *mid*). These values are in good agreement with those in lanthanum sesquioxide (La_2O_3, *A*-type), in which interatomic distances of 237–273 pm occur for *C.N.* = 7 [22]. The $[(La1,2)O_8]^{13-}$ polyhedra are linked by four common edges each in such a way that infinite layers parallel to the *bc* plane are formed, satisfying the Niggli formula $^2_\infty\{[LaO^e_{8/2}]^{5-}\}$ (Figure 5). According to the crystallographic multiplicities, each $(La1)^{3+}$-centered polyhedron is surrounded by four $(La2)^{3+}$-centered ones, but each $(La2)^{3+}$-centered polyhedron is surrounded by two $(La1)^{3+}$- and two $(La2)^{3+}$-centered ones.

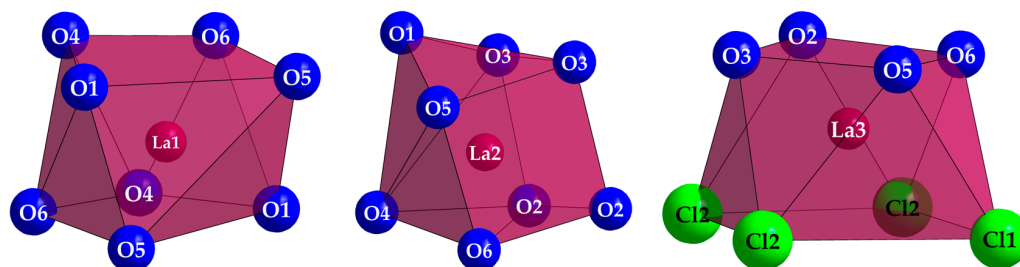**Figure 4.** The square $[LaO_8]^{13-}$ antiprisms or hemiprisms of the $(La1)^{3+}$ and $(La2)^{3+}$ cations in the crystal structure of $La_5Cl_3[SbO_3]_4$ (*left* and *mid*) and the square antiprism $[LaO_4Cl_4]^{9-}$ of the $(La3)^{3+}$ cation (*right*).

In contrast, the third La^{3+} cation also has a coordination number of eight but is coordinated by four oxygen atoms and four Cl⁻ anions in the center of a square antiprism $[(La3)O_4Cl_4]^{9-}$ (Figure 4, *right*). The values of the interatomic distances are d(La3–O) = 232–245 pm and d(La3–Cl) = 323–326 pm, so the lengths of the lanthanum–oxygen bonds are more similar to those in the lanthanum oxide chloride LaOCl (PbFCl-type, 4×239 pm) [20]. The comparison of the distances to the four Cl⁻ anions also shows better agreement with the five values of 313–321 pm for LaOCl [23] compared to those in the lanthanum trichloride $LaCl_3$ (UCl$_3$-type), which exhibits considerably shorter interatomic distances of 295–296 pm for *C.N.* = 9 [24].
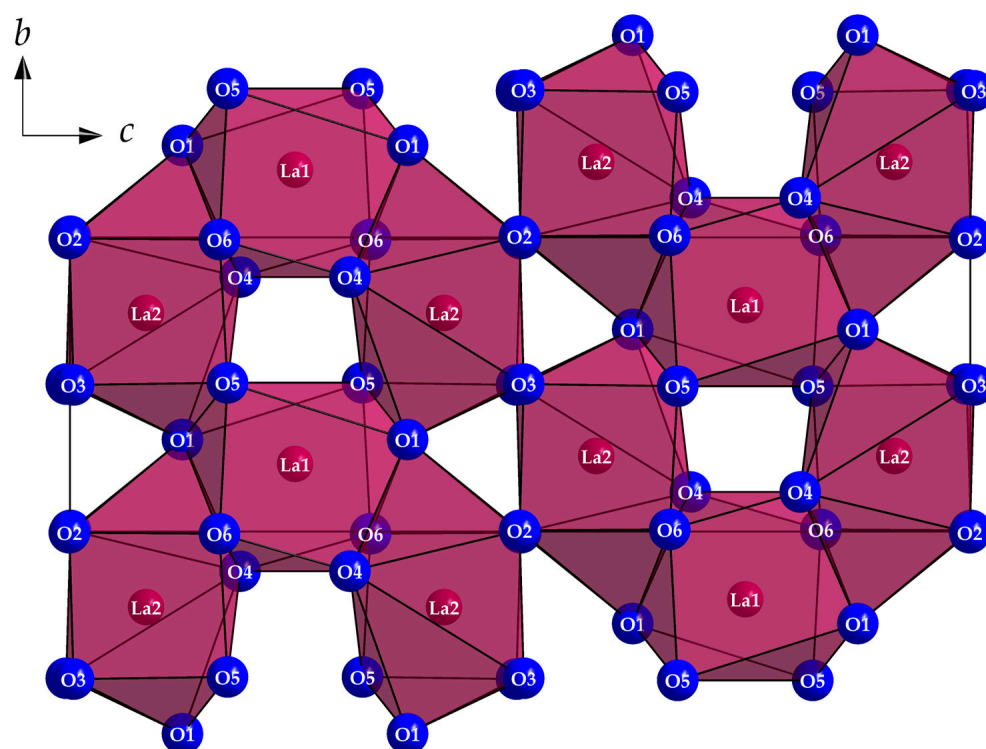
Figure 5. Linkage scheme of the oxygen coordination polyhedra around $(La1)^{3+}$ and $(La2)^{3+}$ in the crystal structure of $La_5Cl_3[SbO_3]_4$ forming a layer with composition $_\infty^2\{[LaO_{8/2}^e]^{5-}\}$ parallel to the *bc*-plane.

The coordination polyhedra around $(La3)^{3+}$ show a different linkage pattern compared to those centered with $(La1)^{3+}$ and $(La2)^{3+}$. Namely, the linkage occurs once via the $(Cl2)^-$ anions, which edge-link the polyhedra along the *b*-axis, forming one-dimensional double strands. A quite similar bonding situation is found in the rare-earth metal(III) halide oxoarsenates(III) $RE_3X_2[As_2O_5][AsO_3]$ (RE = Y, Sm–Gd, Ho–Yb and X = Cl and Br) [3,25]. However, these chains are still corner-linked to each other via the $(Cl1)^-$ anions here, turning the double strands into a two-dimensional bilayer (Figure 6, *top*), which can be described with the Niggli formula $_\infty^2\{[(La3)O_{4/1}^t(Cl1)_{1/2}^v(Cl2)_{3/3}^e]^{6.5-}\}$. The two different Cl^- anions that contribute significantly to the linkage of the $[(La3)O_4Cl_4]^{9-}$ antiprisms are shown again in Figure 6 (*bottom*) in the centers of cationic coordination polyhedra, where the different coordination numbers of *C.N.*(Cl1) = 2 and *C.N.*(Cl2) = 3 are particularly prominent.

The crystal structure of $La_5Cl_3[SbO_3]_4$ exhibits two crystallographically distinct Sb^{3+} cations, both of which actuate a coordination number of *C.N.* = 3 with respect to oxygen atoms to form ψ^1-tetrahedral $[SbO_3]^{3-}$ anions with antimony–oxygen distances of d(Sb1–O) = 196–202 pm and slightly shorter ones of d(Sb2–O) = 187–199 pm (Figure 7). Literature comparison with typical Sb^{3+}–O^{2-} bond lengths reveals values of 198–202 pm for valentinite and senarmontite, the two naturally occurring crystalline modifications of antimony sesquioxide (Sb_2O_3), which are in good agreement [26,27]. With O–Sb–O angles from 83 to 105°, the deflection of the Sb^{3+} cations from the triangular oxygen plane of their trigonal-pyramidal $[SbO_3]^{3-}$ anions amounts to 110–111 pm.
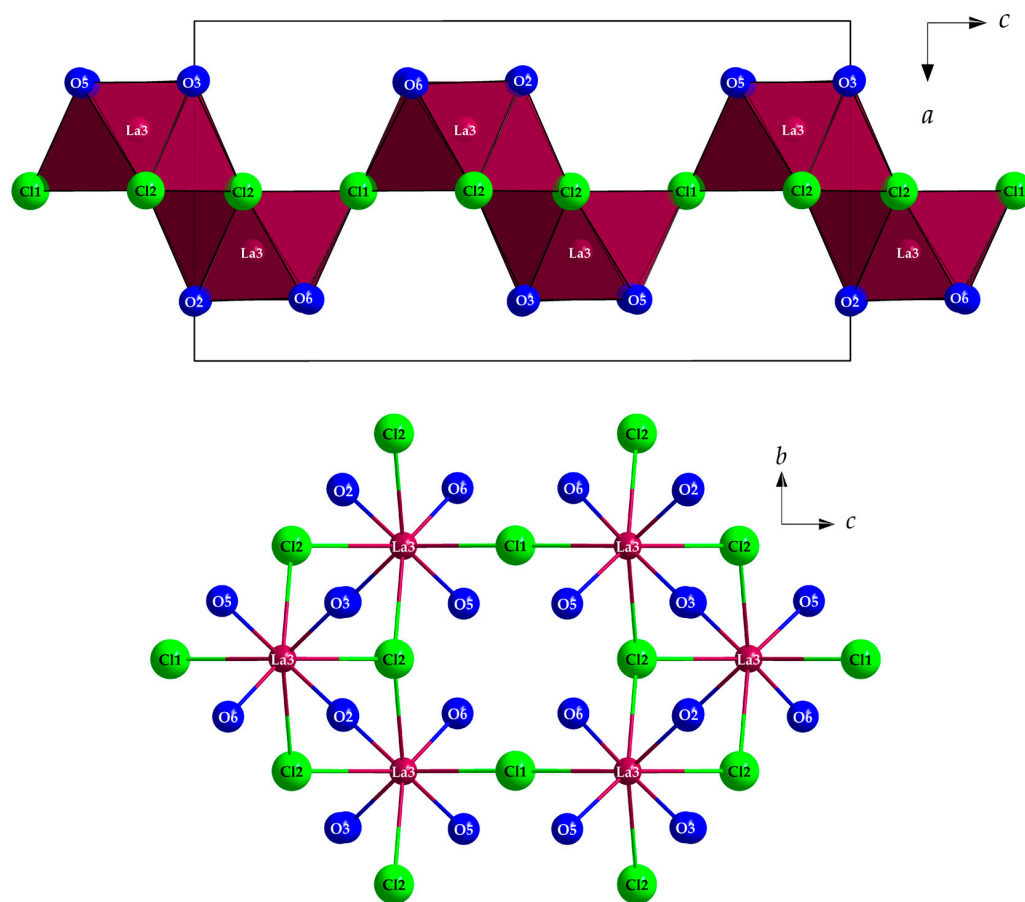
Figure 6. Illustration of the corner- and edge-linkage of the $[(La3)O_4Cl_4]^{9-}$ antiprisms forming layers within the *ac*-plane of the crystal structure of $La_5Cl_3[SbO_3]_4$ (*top*) and function of the two crystallographically independent chloride anions $(Cl1)^-$ and $(Cl2)^-$, and their different coordination environment of $(La3)^{3+}$ cations (*bottom*).

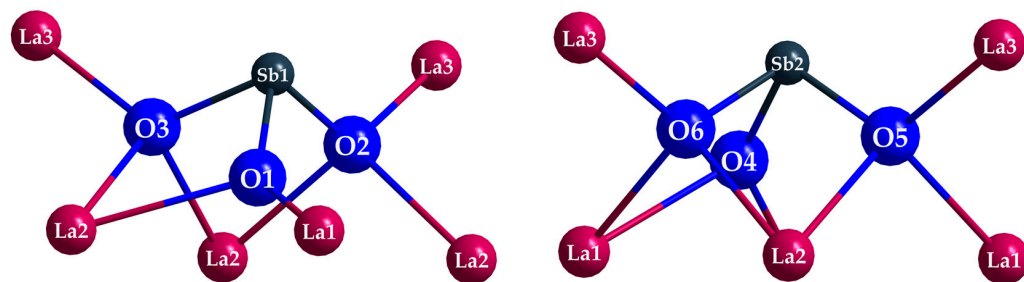**Figure 7.** The two different Sb^{3+} cations in the crystal structure of $La_5Cl_3[SbO_3]_4$ with their first coordination sphere of three oxygen atoms as discrete ψ^1-tetrahedral $[SbO_3]^{3-}$ anions, decorated with La^{3+} cations.

Figure 8 shows a section of the crystal structure of $La_5Cl_3[SbO_3]_4$, emphasizing the cell edges and the different coordination polyhedra. The crystal already showed difficulties in revealing the correct metric during the measurement since an orthorhombic cell was initially suggested due to the measured monoclinic angle of $\beta = 90.007(2)°$. However, only the solution and refinement in the monoclinic space group $P2/c$ provided a reasonable structure model. This refinement was investigated using the software PLATON [28] and the subroutine *Addsym*, which searches for overlooked symmetry operations in the case of higher symmetry structures described in a lower symmetry space group and proposes a higher symmetry space group. However, this algorithm did

not find a more suitable space group, even for a nonfit proportion of about 20%. However, the nearly orthogonal monoclinic angle and the refined twin proportions of about 60% for the major specimen and 40% for the minor one suggest that a higher-symmetric orthorhombic high-temperature modification might exist and that a symmetry break to the monoclinic structure occurs during the course of synthesis upon cooling.
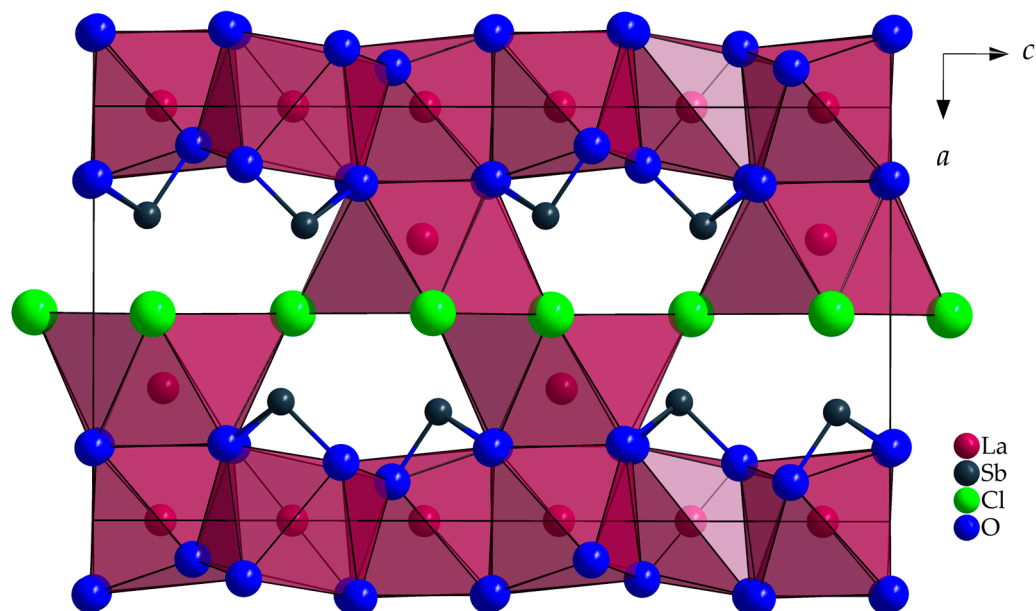

Figure 8. Crystal structure of $La_5Cl_3[SbO_3]_4$ showing unit-cell edges and the coordination polyhedra of the La^{3+} cations.

In contrast to $La_5Cl_3[SbO_3]_4$, which finds its analogy in the rare-earth metal(III) oxoarsenates(III) $Ln_5Br_3[AsO_3]_4$ (Ln = Pr, Sm, Eu, and Tb) [2,3,6], $La_5F_3[SbO_3]_4$ [7] crystallizes isotypically to the rare-earth metal(III) fluoride oxoarsenates(III) $RE_5F_3[AsO_3]_4$ (RE = Y, Ho, Tm–Lu) [2,3] in the tetragonal space group $P4/ncc$ with a = 1208 pm and c = 1144 pm (c/a = 0.947) for Z = 4. Although $La_5F_3[SbO_3]_4$ and $La_5Cl_3[SbO_3]_4$ share the same structured molecular formula, they thus have little in common, except for their discrete ψ^1-tetrahedral $[SbO_3]^{3-}$ and two differently coordinated X^- anions (*C.N.*(F1) = 5 + 1, *C.N.*(F2) = 2), starting with the coordination spheres of the La^{3+} cations. While three La^{3+}-cation positions are present in $La_5Cl_3[SbO_3]_4$, of which only $(La3)^{3+}$ has direct contact with four Cl^- anions according to $[(La3)Cl_4O_4]^{9-}$, two lanthanum sites can be found in $La_5F_3[SbO_3]_4$, which both have contact to F^- anions. The $(La1)^{3+}$ cation is coordinated by eight oxygen atoms in the shape of a square hemiprism with one square face capped by the $(F1)^-$ anion at a distance of 257 pm. Another $(F1)^-$ anion is located above the opposite square face, but it has a distance of 314 pm, which no longer corresponds to a significant chemical bond (Figure 9, *left*). The $(La2)^{3+}$ cations are surrounded by six O^{2-} and two F^- anions each, arranged as a bicapped trigonal prism (Figure 9, *right*). At the same time, the prism is spanned by one $(F2)^-$, one $(O1)^{2-}$, two $(O2)^{2-}$ and two $(O3)^{2-}$ anions, while another $(O1)^{2-}$ and one $(F1)^-$ anion recruit the caps. Therefore, in $La_5F_3[SbO_3]_4$, a three-dimensionally cross-linked network is present, whereas for $La_5Cl_3[SbO_3]_4$, a layered structure occurs.
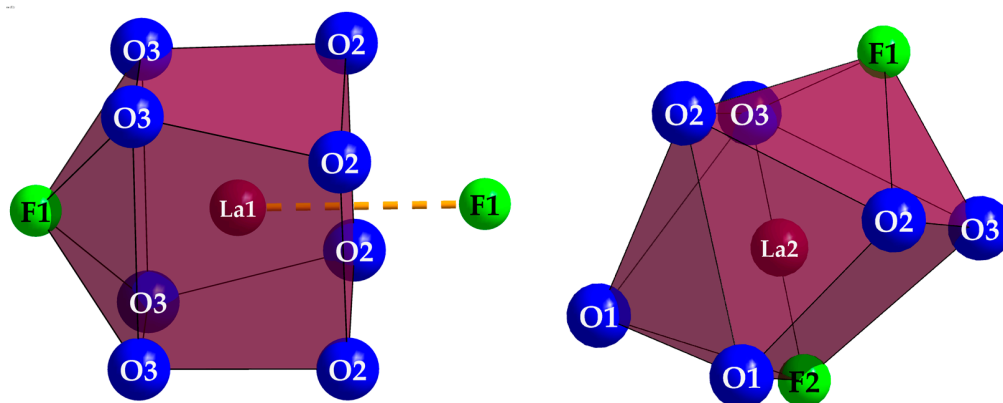
Figure 9. Bicapped square hemiprism $[(La1)O_8F_{(1+1)}]^{15-}$ (*left*) and bicapped trigonal prism $[(La2)O_6F_2]^{11-}$ (*right*) in the tetragonal crystal structure of $La_5F_3[SbO_3]_4$.

The crystallographic data of $La_5Cl_3[SbO_3]_4$ and other parameters, such as fractional atomic coordinates and selected bond lengths, are summarized in Tables 1–3.

3.2. Raman Spectroscopy on $La_5Cl_3[SbO_3]_4$

A single-crystal Raman measurement was performed for further characterization to prove the relationship to the rare-earth metal(III) bromide oxoarsenates(III) $RE_5Br_3[AsO_3]_4$ (*RE* = Pr, Sm, Eu, Tb) [2,3,6]. The spectrum recorded at an excitation wavelength of $\lambda = 638$ nm is shown in Figure 10.

Table 1. Crystallographic data of $La_5Cl_3[SbO_3]_4$ and their determination.

Compound	$La_5Cl_3[SbO_3]_4$
Crystal system	monoclinic
Space group	$P2/c$ (no. 13)
Lattice parameters, a/pm	895.82(5)
b/pm	564.28(3)
c/pm	1728.19(9)
β/°	90.007(2)
Number of formula units, Z	2
Calculated density, D_x/g·cm^{-3}	5.626
Molar volume, V_m/cm^3·mol^{-1}	263.05
Diffractometer	κ-CCD (Bruker-Nonius)
Wavelength	$\lambda = 71.07$ pm (Mo-K_α)
Electron sum, $F(000)$/e$^-$	1272
Measurement limit, Θ_{max}/°	27.49
Measurement range ($\pm h_{max}$, $\pm k_{max}$, $\pm l_{max}$)	11, 7, 22
Number of measured reflections	14795
Number of symmetry-independent ones	2015
Absorption coefficient, μ/mm^{-1}	18.52
Absorption correction	Program X-SHAPE 2.21 [18]
R_{int}/ R_σ	0.058/0.031
R_1/R_1 with $|F_o| \geq 4\sigma(F_o)$	0.049/0.037
wR_2/Goodness of Fit (GooF)	0.085/1.093
Structure determination and refinement	Program SHELX-97 [19]
Extinction coefficient, ε/10^{-6} pm^{-3}	0.00075(6)
Residual electron density, $\rho_{max/min}$/e$^-$ 10^{-6} pm^{-3}	4.03/$-$3.89
Batch scale factor (BASF) [1]	0.396(2)
CSD number	2214525

[1] This value represents the percentage of the twin individuum.

Table 2. Fractional atomic coordinates, *Wyckoff* sites, and equivalent isotropic displacement parameters for $La_5Cl_3[SbO_3]_4$.

Atom	Site	x/a	y/b	z/c	U_{eq}/pm^2
La1	2*e*	0	0.2301(3)	$1/4$	248(3)
La2	4*g*	0.00064(9)	0.74327(17)	0.41548(5)	129(2)
La3	4*g*	0.31942(9)	0.24959(17)	0.41245(5)	149(2)
Cl1	2*f*	$1/2$	0.2476(9)	$1/4$	306(14)
Cl2	4*g*	0.4983(4)	0.7512(7)	0.4259(2)	247(8)
Sb1	4*g*	0.26331(11)	0.25317(18)	0.06713(5)	141(2)
Sb2	4*g*	0.28708(11)	0.75412(18)	0.26472(5)	148(3)
O1	4*g*	0.0940(16)	0.313(3)	0.1250(7)	713(51)
O2	4*g*	0.1748(12)	0.004(2)	0.0007(7)	217(22)
O3	4*g*	0.1797(12)	0.499(2)	0.4960(7)	203(22)
O4	4*g*	0.1406(15)	0.865(2)	0.1890(7)	481(38)
O5	4*g*	0.1805(13)	0.506(2)	0.3250(7)	215(27)
O6	4*g*	0.1858(14)	0.993(2)	0.3339(7)	270(33)

Table 3. Selected interatomic distances (d/pm) in $La_5Cl_3[SbO_3]_4$ and bond angles ($\sphericalangle/°$) of the ψ^1-tetrahedral $[SbO_3]^{3-}$ anions.

Bond		d/pm	Bond		d/pm
La1–O1	2×	236.5(13)	Sb1–O1	1×	184.8(14)
La1–O6	2×	258.2(12)	Sb1–O2	1×	198.2(12)
La1–O5	2×	259.1(11)	Sb1–O3	1×	200.9(12)
La1–O1	2×	263.3(13)			
			Sb2–O4	1×	195.7(13)
La2–O4	1×	230.9(12)	Sb2–O5	1×	199.0(12)
La2–O3	1×	253.3(11)	Sb3–O6	1×	201.6(11)
La2–O2	1×	257.6(11)			
La2–O6	1×	259.3(13)	**Atom triple**		$\sphericalangle/°$
La2–O2′	1×	259.5(12)	O1–Sb1–O2	1×	96.6(8)
La2–O3′	1×	261.0(12)	O2–Sb1–O3	1×	89.5(5)
La2–O5	1×	261.5(11)	O3–Sb1–O1	1×	84.2(7)
La2–O1	1×	266.6(14)			
			O4–Sb2–O5	1×	104.7(6)
La3–O6	1×	231.8(11)	O5–Sb2–O6	1×	86.8(5)
La3–O3	1×	237.2(12)	O6–Sb2–O4	1×	83.1(5)
La3–O5	1×	243.4(12)			
La3–O2	1×	246.0(13)			
La3–Cl2	1×	323.6(4)			
La3–Cl1	1×	324.0(3)			
La3–Cl2′	1×	324.5(4)			
La3–Cl2″	1×	326.0(4)			

The symmetric Sb^{3+}–O^{2-} valence vibration can be identified as the second strongest band, which is located at a wavenumber of about 721 cm^{-1} for $La_5Cl_3[SbO_3]_4$. The band found at 621 cm^{-1} has a much lower intensity and can be assigned to asymmetric valence vibration. The other bands at 523 and 462 cm^{-1} belong to the symmetric and at 388, 327, and 296 cm^{-1} to the asymmetric deformation vibrations. Finally, at 212 and 145 cm^{-1}, the lattice vibrations occur. Compared to the rare-earth metal(III) bromide oxoarsenates(III) $RE_5Br_3[AsO_3]_4$, the spectrum is almost the same, but the peaks are much better defined and only shifted by a few wavenumbers [29,30]. As with the rare-earth metal(III) oxoantimonate(III) chlorides of composition $RESb_2O_4Cl$ (RE = Y, Sm–Lu) [3,6,12–14], the common mode valence vibration of the terminal oxygen atoms to the antimony is similarly pronounced at about 700–720 cm^{-1}. However, $La_5Cl_3[SbO_3]_4$ lacks the push-pull vibration,

which is found in the range of 660 cm^{-1} for $GdSb_2O_4Cl$ and at 672 cm^{-1} for $SmSb_2O_4Cl$, since the latter contains discrete $[Sb_4O_8]^{4-}$ rings of four cyclically vertex-connected ψ^1-tetrahedral $[SbO_3]^{3-}$ units according to $RE_2[Sb_4O_8]Cl_2$ [3,6,12–14].

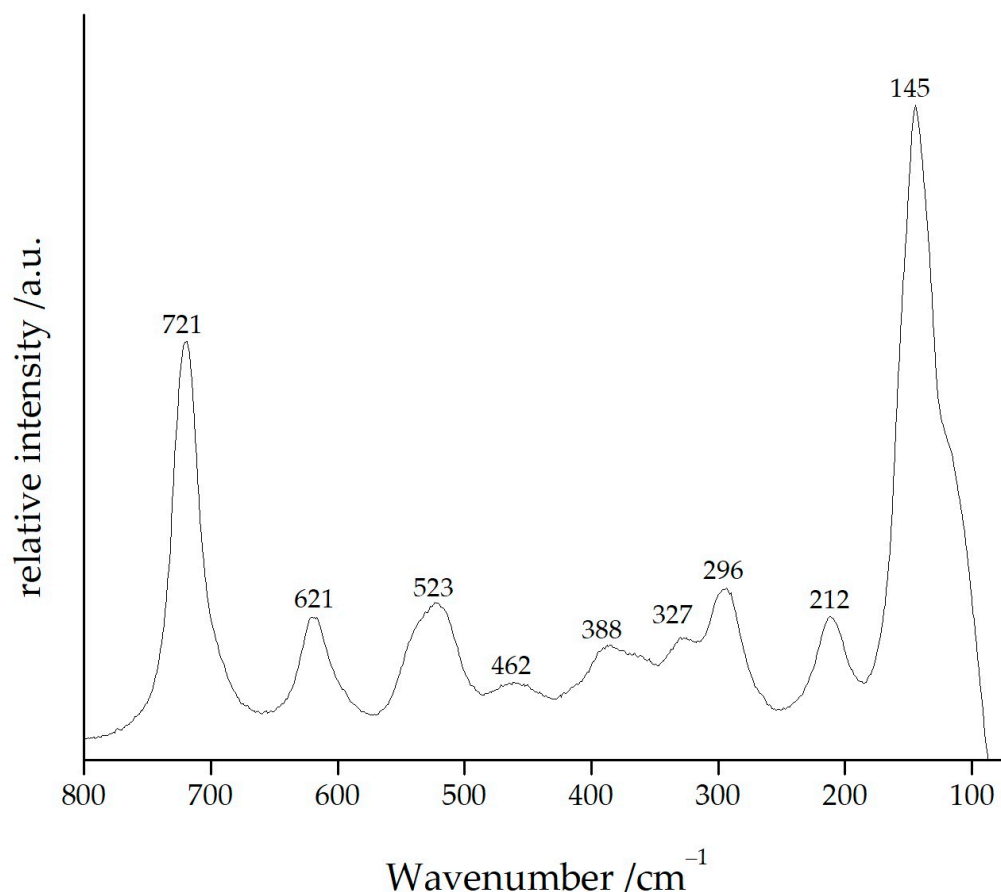**Figure 10.** Single-crystal Raman spectrum of $La_5Cl_3[SbO_3]_4$ (excitation wavelength: $\lambda = 638$ nm).

3.3. Crystal Structure of $La_2Sb_{12}O_{19}Br_4$ and $La_2Sb_{12}O_{19}I_4$

Synthesis experiments to prepare $LaSb_2O_4Br$ and $LaSb_2O_4I$ have failed so far but yielded two isostructural lanthanum oxoantimonate(III) halides with the composition $La_2Sb_{12}O_{19}X_4$ (X = Br and I). Both crystallize orthorhombically in the space group *Pnma* with $Z = 2$. The unit-cell parameters for the bromide are $a = 3184.69(19)$ pm, $b = 417.78(3)$ pm, $c = 1019.85(6)$ pm, while for the iodide, they amount to $a = 3215.08(19)$ pm, $b = 419.94(3)$ pm, $c = 1062.89(6)$ pm, so as expected, the iodide shows larger values as compared to the bromide owing to the larger radius of the iodide anion ($r_i(I^-) = 220$ pm) versus $r_i(Br^-) = 195$ pm). One of the characteristic structural features of these compounds becomes apparent when considering the environment of the unique La^{3+} cation. This crystallographically singular cation is coordinated by nine oxygen atoms arranged as a capped square antiprism. These $[LaO_9]^{15-}$ polyhedra form an endless strand along the *b*-axis according to $\frac{1}{\infty}\{[LaO_{5/1}^{\ t}O_{4/2}^{\ e}]^{11-}\}$, which undergoes linkage via two polyhedral edges (2 × O4···O7). The lanthanum–oxygen distances fall into the range of $d(La–O) = 239–297$ pm for the bromide and $d(La–O) = 240–296$ pm for the iodide derivative (Figure 11). These numbers agree quite well with literature values of $d(La–O) = 237–273$ pm for C.N. = 7 in *A*-type La_2O_3 [22] and even better with PbFCl-type LaOBr ($d(La–O) = 240$ pm) [31] and LaOI ($d(La–O) = 241$ pm) [32] although there are no X^- anions in the coordination sphere of La^{3+} in the $La_2Sb_{12}O_{19}X_4$ cases.
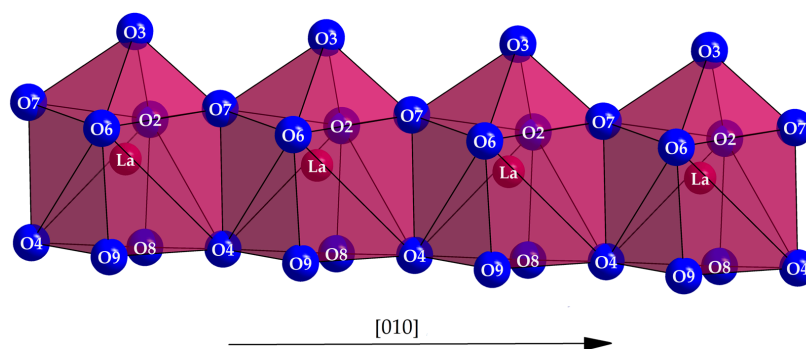
Figure 11. Strand of edge-linked isotactically aligned $[LaO_9]^{15-}$ polyhedra according to ${}^1_\infty\{[LaO^t_{5/1}O^e_{4/2}]^{11-}\}$ in the crystal structure of $La_2Sb_{12}O_{19}Br_4$ and $La_2Sb_{12}O_{19}I_4$.

Another substructure within these compounds is that of the antimony–oxygen environment. Most of the Sb^{3+} cations, together with four oxygen atoms, form trigonal ψ^1_{eq}-bipyramids $[SbO_4]^{5-}$ (Sb1–Sb5, Figure 12), which are linked to each other either by an edge (Sb2 with Sb3 and Sb1 with Sb4) or by a corner (Sb1 with Sb3 and Sb5 with Sb4, as well as Sb5 with Sb6). In contrast, the $(Sb6)^{3+}$ cations form ψ^1-tetrahedra $[SbO_3]^{3-}$ (Figure 12) with only three oxygen atoms each, which in turn are linked to one another via edges (O6···O6). The oxygen atom O7 remains terminal, and both O6 atoms link two open "halfpipes" with two $(Sb6)^{3+}$ cations each as linkers to form a "double-halfpipe" ${}^1_\infty\{[Sb_{12}O_{19}]^{2-}\}$ (Figure 12). Within these so-called "double-halfpipes", the antimony–oxygen distances range from 197 to 225 pm (*plus* 254 pm) for $La_2Sb_{12}O_{19}Br_4$ and from 192 to 227 pm (*plus* 256 pm) for $La_2Sb_{12}O_{19}I_4$, which agree quite well with literature values of $d(Sb–O) = 198–202$ pm (*plus* 251 and 262 pm) in valentinite (β-Sb_2O_3) [27] and come slightly higher than $d(Sb–O) = 198$ pm ($3\times$) in senarmontite (α-Sb_2O_3) [26], but show a high degree of diversity.
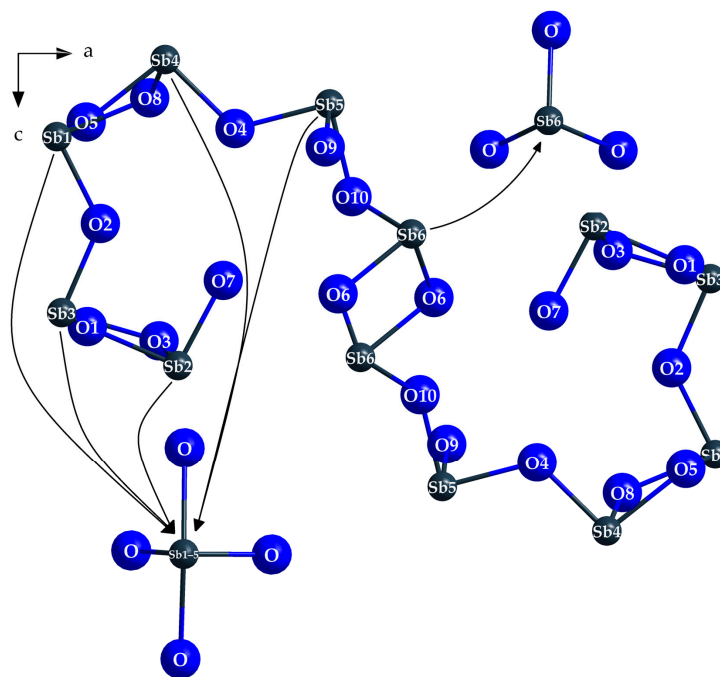
Figure 12. Condensed trigonal ψ^1_{eq}-bipyramids $[SbO_4]^{5-}$ (with Sb1–Sb5) and ψ^1-tetrahedra $[SbO_3]^{3-}$ (with Sb6) forming "double-halfpipes" ${}^1_\infty\{[Sb_{12}O_{19}]^{2-}\}$, which run along [010] and consist of two "half-pipes" linked via O6 ($2\times$) at Sb6 in the crystal structure of $La_2Sb_{12}O_{19}Br_4$ and $La_2Sb_{12}O_{19}I_4$. An inversion center is notable within the central (Sb6)–(O6)···(O6)–(Sb6) rhombuses.

The capped square hemiprisms $[LaO_9]^{15-}$ are located within these "double-halfpipes", where each oxygen atom of every $[LaO_9]^{15-}$ polyhedron is also a component of the antimony-oxygen "double-halfpipe" arrangement (Figure 13).
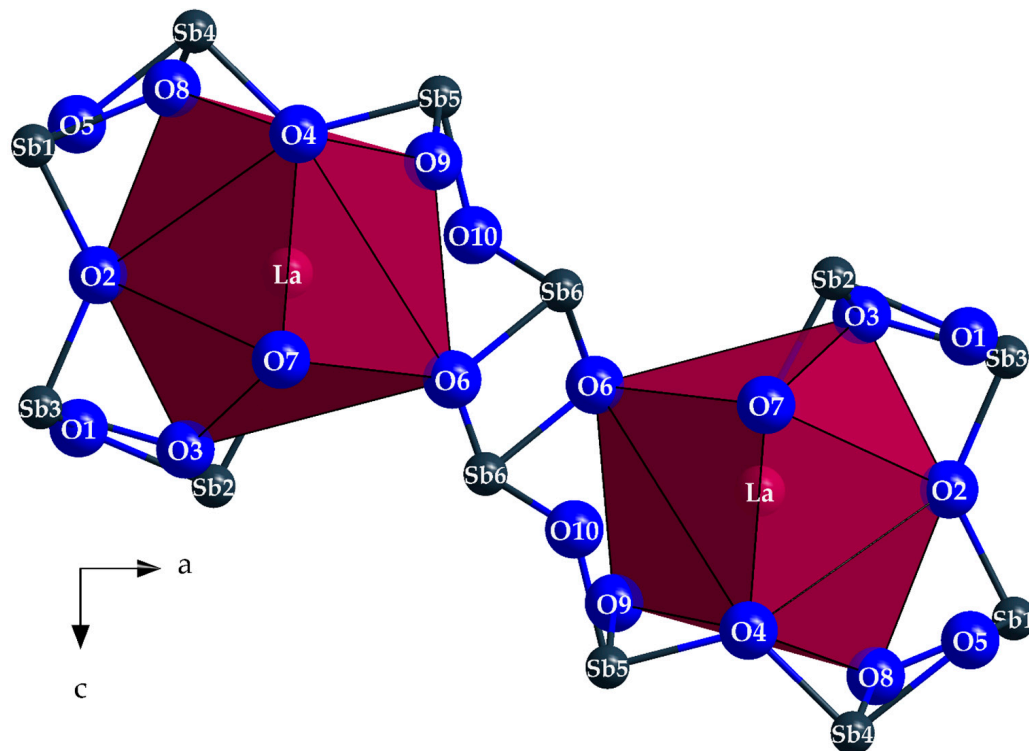

Figure 13. Environment of the edge-linked $[LaO_9]^{15-}$ polyhedra within the "double-halfpipes" $^1_\infty\{[Sb_{12}O_{19}]^{2-}\}$ of antimony and oxygen in the crystal structure of $La_2Sb_{12}O_{19}Br_4$ and $La_2Sb_{12}O_{19}I_4$.

Furthermore, the environment of the heavy halide anions X^- (X = Br and I) is also very interesting. $(X1)^-$ is surrounded by ten Sb^{3+} cations with the shape of a bicapped square prism, while $(X2)^-$ has nine Sb^{3+} cations arranged as monocapped square prisms as nearest neighbors. Therefore, once again, no bonding $La^{3+}\cdots X^-$ contacts occur since the shortest $La^{3+}\cdots X^-$ distances are 332 pm for X = Br and 342 pm for X = I. There are always two of these prisms $[(X1)Sb_{10}]^{29+}$ and $[(X2)Sb_9]^{26+}$ linked together to form a double unit via a shared face ($2\times$ Sb2 + $2\times$ Sb4). Figure 14 also shows that the $(Sb6)^{3+}$ cations can be present only in half of their abundance in both cases to avoid too short distances between two of them (110 pm for X = Br, 104 pm for X = I) at the corresponding corners of each $[(X2)Sb_9]^{26+}$ polyhedron. The antimony–halide distances range from 332 to 375 pm for $La_2Sb_{12}O_{19}Br_4$ and from 342 to 385 pm for $La_2Sb_{12}O_{19}I_4$, so one can not speak of real chemical bonds here, but only of long secondary contacts.

The content of an extended unit cell of the crystal structure of both $La_2Sb_{12}O_{19}X_4$ representatives (X = Br and I) as viewed along [010] can be seen in Figure 15, which suggests the impression of a hexagonal packing of rods or better "double-halfpipes" $^1_\infty\{[Sb_{12}O_{19}]^{2-}\}$, encapsulating the La^{3+} cations to form one $^1_\infty\{[LaO_{5/1}^{\,t}O_{4/2}^{\,e}]^{11-}\}$ strand per "halfpipe".

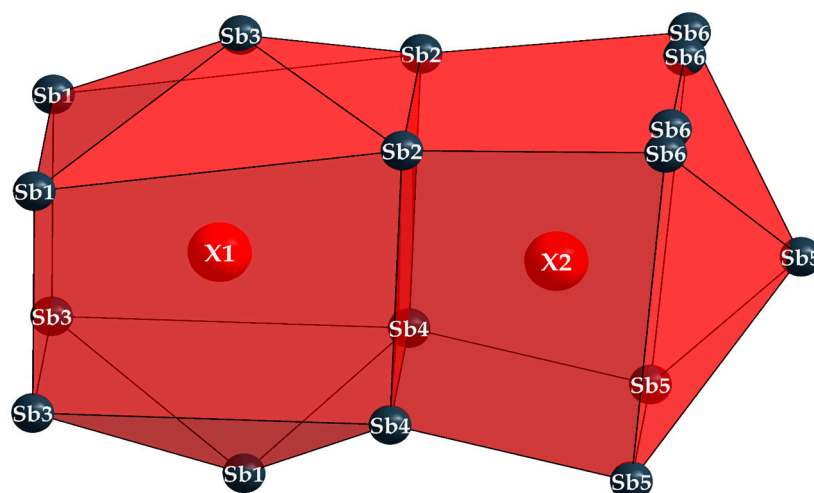**Figure 14.** Cationic environment of the X^- anions within the crystal structure of both $La_2Sb_{12}O_{19}X_4$ representatives (X = Br and I) with mono- and bicapped square prisms of Sb^{3+} cations, respectively.
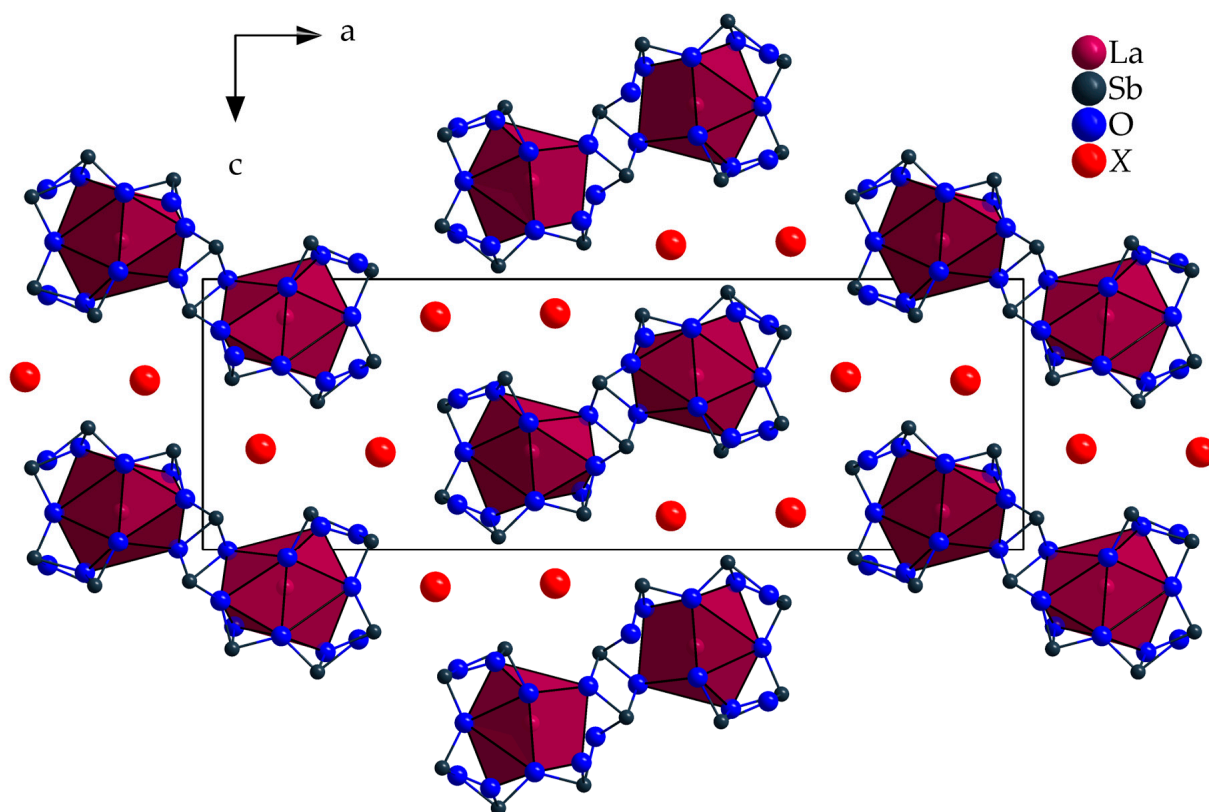
Figure 15. Extended unit cell of the crystal structure of both $La_2Sb_{12}O_{19}X_4$ representatives (X = Br and I) as viewed along [010].

Tubular or semi-tubular arrangements of antimony and oxygen are not so rare, especially when heavy anions (X^- = Br$^-$ and I$^-$) occur in antimony(III) oxide halides, such as $Sb_8O_{11}X_2$ (X = Cl–I) [33–35], Sb_5O_7I [36–38], and Sb_3O_4I [39]. Even with additional alkali-metal cations, they persist, for example, in the systems $AI_4RE_2Sb_{8.333}O_{14}$ (A = K–Cs; RE = Y, Pr–Tm) [6,20,21].

The crystallographic data of $La_2Sb_{12}O_{19}Br_4$ and $La_2Sb_{12}O_{19}I_4$ and other parameters, such as fractional atomic coordinates and selected bond lengths, are summarized in Tables 4–7.

Table 4. Crystallographic data of $La_2Sb_{12}O_{19}Br_4$ and $La_2Sb_{12}O_{19}I_4$ and their determination.

Compound	$La_2Sb_{12}O_{19}Br_4$	$La_2Sb_{12}O_{19}I_4$
Crystal system	orthorhombic	
Space group	*Pnma* (no. 62)	
Lattice parameters, a/pm	3184.69(19)	3215.08(19)
b/pm	417.78(3)	419.94(3)
c/pm	1019.85(6)	1062.89(6)
Number of formula units, Z	2	
Calculated density, D_x/g·cm^{-3}	5.782	5.902
Molar volume, V_m/cm^3·mol^{-1}	408.60	432.15
Diffractometer	STADI-VARI (Stoe & Cie)	κ-CCD (Bruker-Nonius)
Wavelength	λ = 56.08 pm (Ag-K_α)	λ = 71.07 pm (Mo-K_α)
Electron sum, $F(000)$/e$^-$	2036	2180
Measurement limit, Θ_{max}/°	30.66	27.48
Measurement range ($\pm h_{max}$, $\pm k_{max}$, $\pm l_{max}$)	57, 7, 18	41, 5, 13
Number of measured reflections	33659	22948
Number of symmetry-independent ones	4554	1873
Absorption coefficient, μ/mm^{-1}	11.01	18.37
Absorption correction	Program X-SHAPE 2.21 [18]	
R_{int}/ R_σ	0.069/0.059	0.175/0.092
R_1/R_1 with $|F_o| \geq 4\sigma(F_o)$	0.104/0.066	0.119/0.063
wR_2/Goodness of Fit (GooF)	0.173/1.043	0.161/0.985
Structure determination and refinement	Program SHELX-97 [19]	
Residual electron density, $\rho_{max/min}$/e$^-$ 10^{-6} pm^{-3}	7.77/−7.31	5.50/−3.18
CSD number	2250889	2250901

Table 5. Fractional atomic coordinates, *Wyckoff* sites, and equivalent isotropic displacement parameters of $La_2Sb_{12}O_{19}Br_4$.

Atom	Site	s.o.f.	x/a	y/b	z/c	U_{eq}/pm^2
La	4c	1	0.40012(2)	$^1/_4$	0.64836(6)	147(1)
Sb1	4c	1	0.29137(2)	$^1/_4$	0.81595(8)	183(2)
Sb2	4c	1	0.13081(2)	$^1/_4$	0.86234(7)	130(1)
Sb3	4c	1	0.29463(2)	$^1/_4$	0.46716(7)	127(1)
Sb4	4c	1	0.13980(3)	$^1/_4$	0.47176(8)	279(2)
Sb5	4c	1	0.03442(3)	$^1/_4$	0.38192(9)	332(2)
Sb6	8d	0.500(3) [a]	0.01684(3)	0.1180(4)	0.87741(12)	269(4)
O1	4c	1	0.1884(2)	$^1/_4$	0.9352(8)	146(12)
O2	4c	1	0.3206(3)	$^1/_4$	0.6449(8)	186(14)
O3	4c	1	0.3562(2)	$^1/_4$	0.4099(8)	153(13)
O4	4c	1	0.0953(3)	$^1/_4$	0.3314(10)	240(17)
O5	4c	1	0.1887(3)	$^1/_4$	0.3465(10)	262(18)
O6	4c	1	0.4700(3)	$^1/_4$	0.5066(9)	225(16)
O7	4c	1	0.1027(2)	$^1/_4$	0.0347(8)	173(14)
O8	4c	1	0.3506(3)	$^1/_4$	0.8952(11)	309(20)
O9	4c	0.73(4) [b]	0.4643(5)	$^1/_4$	0.8020(16)	383(52)
O10	4c	0.77(4) [b]	0.0204(5)	$^1/_4$	0.1941(16)	442(49)
Br1	4c	1	0.27927(5)	$^1/_4$	0.14307(13)	318(3)
Br2	4c	1	0.43006(4)	$^1/_4$	0.12576(14)	302(3)

[a] freely refined fractional site occupation factor (s.o.f.); [b] constraintly refined site occupation factors with s.o.f.(O9) + s.o.f.(O10) = 1.5.

Table 6. Fractional atomic coordinates, *Wyckoff* sites, and equivalent isotropic displacement parameters of $La_2Sb_{12}O_{19}I_4$.

Atom	Site	s.o.f.	x/a	y/b	z/c	U_{eq}/pm^2
La	4c	1	0.39978(5)	$1/4$	0.64015(13)	165(4)
Sb1	4c	1	0.29170(5)	$1/4$	0.80393(14)	186(4)
Sb2	4c	1	0.13171(5)	$1/4$	0.86652(14)	145(4)
Sb3	4c	1	0.29476(5)	$1/4$	0.46760(14)	132(4)
Sb4	4c	1	0.13978(6)	$1/4$	0.45113(15)	279(5)
Sb5	4c	1	0.03568(6)	$1/4$	0.36641(16)	370(6)
Sb6	8d	0.500(4) [a]	0.01618(7)	0.1258(6)	0.88214(19)	275(8)
O1	4c	1	0.1888(5)	$1/4$	0.9406(14)	170(40)
O2	4c	1	0.3194(6)	$1/4$	0.6373(14)	278(45)
O3	4c	1	0.3563(5)	$1/4$	0.4150(14)	188(38)
O4	4c	1	0.0953(5)	$1/4$	0.3193(16)	288(46)
O5	4c	1	0.1897(6)	$1/4$	0.3309(17)	361(49)
O6	4c	1	0.4694(5)	$1/4$	0.5037(16)	257(42)
O7	4c	1	0.1029(5)	$1/4$	0.0307(15)	223(41)
O8	4c	1	0.3505(6)	$1/4$	0.8757(18)	489(60)
O9	4c	0.74(5) [b]	0.4614(8)	$1/4$	0.786(3)	916(167)
O10	4c	0.76(5) [b]	0.0214(8)	$1/4$	0.191(2)	788(142)
I1	4c	1	0.28347(5)	$1/4$	0.13865(14)	224(4)
I2	4c	1	0.42943(6)	$1/4$	0.12643(15)	294(5)

[a] freely refined fractional site occupation factor (*s.o.f.*); [b] constraintly refined site occupation factors with *s.o.f.*(O9) + *s.o.f.*(O10) = 1.5.

3.4. Raman Spectroscopy on $La_2Sb_{12}O_{19}I_4$

The Raman spectrum of $La_2Sb_{12}O_{19}I_4$, shown in Figure 16, was recorded at an excitation wavelength of λ = 532 nm. At a wavenumber of 627 cm^{-1}, the push-pull valence vibration can be seen, which is much more pronounced in contrast to the chloride derivatives $RESb_2O_4Cl$ (*RE* = Y, Sm–Lu) [3,6,12–14], while the valence vibration in the common mode can not be detected in the spectrum at all. This is due to the presence of isolated $[Sb_4O_8]^{4-}$-ring units consisting of four vertex-connected ψ^1-tetrahedra $[SbO_3]^{3-}$ in the $RESb_2O_4Cl$ examples, while in $La_2Sb_{12}O_{19}I_4$ and $La_2Sb_{12}O_{19}Br_4$, endless "double-halfpipes" of antimony and oxygen with mostly tetracoordinated Sb^{3+} cations are encountered. Furthermore, the peaks at 511 and 479 cm^{-1} can be assigned to the symmetric deformation vibrations of the vast minority of ψ^1-tetrahedra $[SbO_3]^{3-}$. At 201, 144, 108, 74, and 61 cm^{-1}, several bands are found, which probably belong to lattice vibrations [29,30].

Table 7. Selected interatomic distances (d/pm) in La$_2$Sb$_{12}$O$_{19}$Br$_4$ (*left*) and La$_2$Sb$_{12}$O$_{19}$I$_4$ (*right*).

Bond		d/pm	Bond		d/pm
La–O2	1×	253.3(9)	La–O2	1×	258.5(19)
La–O3	1×	280.6(8)	La–O3	1×	277.2(15)
La–O4	2×	280.5(7)	La–O4	2×	283.9(12)
La–O6	1×	265.3(9)	La–O6	1×	266.8(16)
La–O7	2×	239.1(4)	La–O7	2×	240.2(8)
La–O8	1×	297.1(11)	La–O8	1×	296.4(19)
La–O9	1×	257.5(16)	La–O9	1×	252(2)
Sb1–O2	1×	197.7(8)	Sb1–O2	1×	198.2(17)
Sb1–O5	2×	220.5(3)	Sb1–O5	2×	220.2(5)
Sb1–O8	1×	205.3(9)	Sb1–O8	1×	203.7(19)
Sb2–O1	1×	198.0(7)	Sb2–O1	1×	199.8(16)
Sb2–O3	2×	218.4(2)	Sb2–O3	2×	219.6(4)
Sb2–O7	1×	197.2(8)	Sb2–O7	1×	197.6(15)
Sb3–O1	2×	218.2(2)	Sb3–O1	2×	218.4(4)
Sb3–O2	1×	199.2(8)	Sb3–O2	1×	197.0(14)
Sb3–O3	1×	204.6(7)	Sb3–O3	1×	205.5(15)
Sb4–O4	1×	201.4(9)	Sb4–O4	1×	200.3(15)
Sb4–O5	1×	201.4(9)	Sb4–O5	1×	205.3(17)
Sb4–O8	2×	225.1(4)	Sb4–O8	2×	226.9(7)
Sb5–O4	1×	200.7(8)	Sb5–O4	1×	198.0(18)
Sb5–O9	2×	224.3(6)	Sb5–O9	2×	226.9(13)
Sb5–O10	1×	196.7(16)	Sb5–O10	1×	192(3)
Sb6–O6	1×	198.1(8)	Sb6–O6	1×	200.1(16)
Sb6–O6′	1×	206.8(6)	Sb6–O6′	1×	209.2(11)
Sb6⋯O9	1×	254.1(17)	Sb6⋯O9	1×	256(3)
Sb6–O10	1×	207.5(11)	Sb6–O10	1×	213.7(19)
Sb1⋯Br1	1×	335.80(16)	Sb1⋯I1	1×	356.8(2)
Sb1⋯Br1′	2×	354.09(13)	Sb1⋯I1′	2×	356.2(2)
Sb2⋯Br2	2×	373.39(13)	Sb2⋯I2	2×	384.6(2)
Sb3⋯Br1	1×	334.11(13)	Sb3⋯I1	1×	351.5(2)
Sb3⋯Br1′	2×	362.23(13)	Sb3⋯I1′	2×	374.7(2)
Sb4⋯Br1	2×	374.84(15)	Sb4⋯I1	2×	380.4(2)
Sb4⋯Br2	2×	343.24(13)	Sb4⋯I2	2×	358.3(2)
Sb5⋯Br2	1×	332.45(16)	Sb5⋯I2	1×	341.6(3)
Sb5⋯Br2′	2×	343.91(13)	Sb5⋯I2′	2×	364.8(2)
Sb6⋯Br2	1×	343.68(18)	Sb6⋯I2	1×	359.6(3)

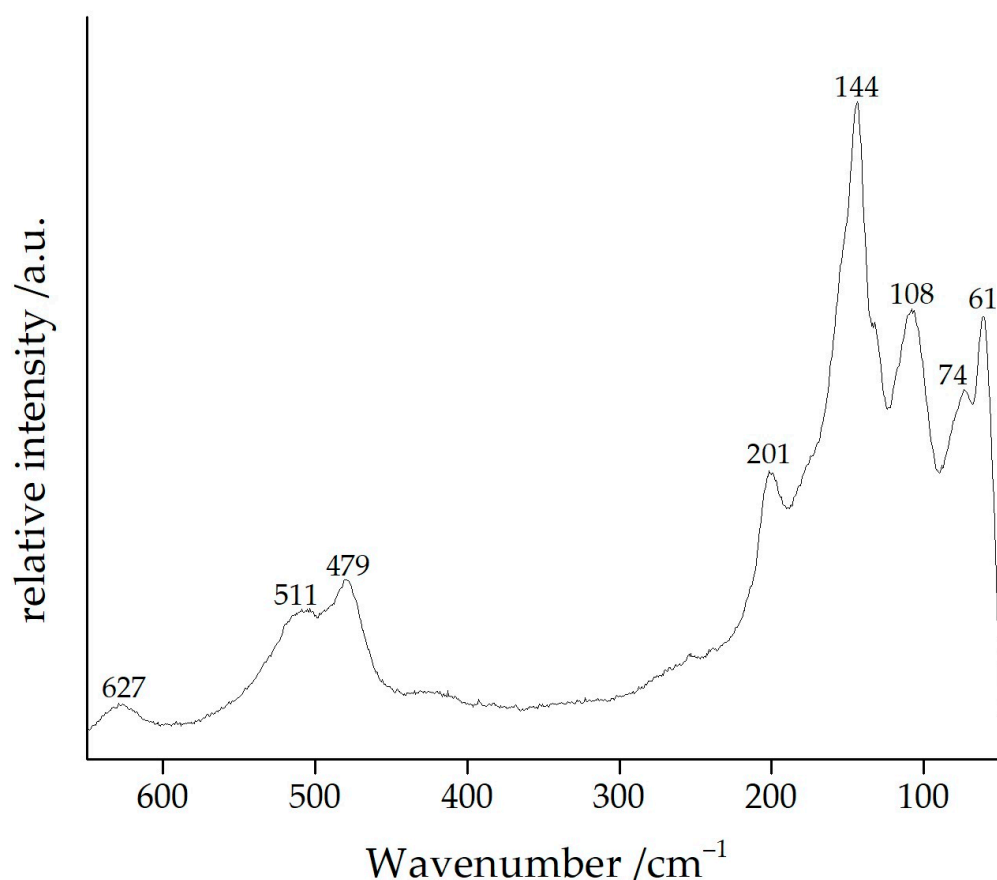**Figure 16.** Single-crystal Raman spectrum of $La_2Sb_{12}O_{19}I_4$ (excitation wavelength: λ = 532 nm).

4. Conclusions

With the three new compounds presented here, the spectrum of lanthanum oxoantimonate(III) halides has been considerably extended. It was possible to obtain colorless single crystals of all three (monoclinic $La_5Cl_3[SbO_3]_4$ as well as orthorhombic $La_2Sb_{12}O_{19}Br_4$ and $La_2Sb_{12}O_{19}I_4$) and to determine their crystal structures. Furthermore, Raman measurements were performed on both structure types and compared with known rare-earth metal(III) oxoantimonate(III) halides with the composition $RESb_2O_4X$. Moreover, a structural comparison of tetragonal $La_5F_3[SbO_3]_4$ with three-dimensional and monoclinic $La_5Cl_3[SbO_3]_4$ with two-dimensional expression was performed, where differences and similarities could be worked out. According to X-ray powder investigations, there are more phases to consider (e.g., $La_5Br_3[SbO_3]_4$ with laminar and $CsI_4La_2Sb_{8.333}O_{14}$ with tubular structure characteristics, such as $La_2Sb_{12}O_{19}Br_4$ and $La_2Sb_{12}O_{19}I_4$), so further studies into the La–Sb–O–X systems seem to be necessary.

Author Contributions: Conceptualization, R.J.C.L. and T.S.; methodology, R.J.C.L., K.-N.B. and F.C.G.; software, R.J.C.L.; validation, T.S.; formal analysis, R.J.C.L. and F.C.G.; investigation, R.J.C.L. and F.C.G.; resources, T.S.; data curation, R.J.C.L., F.C.G. and T.S.; writing—original draft preparation, R.J.C.L., K.-N.B. and F.C.G.; writing—review and editing, R.J.C.L. and T.S.; visualization, R.J.C.L.; supervision, T.S.; project administration, T.S.; funding acquisition, T.S. All authors have read and agreed to the published version of the manuscript.

Institutional Review Board Statement: Not applicable.

Informed Consent Statement: Not applicable.

References

1. Ledderboge, F.; Schleid, T. The First Lanthanoid(III) Fluoride Oxoarsenate(III): $Lu_5F_3[AsO_3]_4$. *Z. Anorg. Allg. Chem.* **2014**, *640*, 2351.
2. Ledderboge, F. Synthese und Charakterisierung von Oxo- und Thioarsenaten(III/V) der Seltenerdmetalle und derer Derivate. Ph.D. Thesis, University of Stuttgart, Stuttgart, Germany, 2016.
3. Goerigk, F.C. Synthese und Charakterisierung von Seltenerdmetall-Oxidoarsenaten und -antimonaten sowie deren Anwendungsbezug. Ph.D. Thesis, University of Stuttgart, Stuttgart, Germany, 2021.
4. Kang, D.-H. Oxoarsenate(III/V) und Thioarsenate(III) der Selten-Erd-Metalle. Ph.D. Thesis, University of Stuttgart, Stuttgart, Germany, 2009.
5. Goerigk, F.C.; Schander, S.; Hamida, M.B.; Kang, D.-H.; Ledderboge, F.; Wickleder, M.S.; Schleid, T. Die monoklinen Seltenerdmetall(III)-Chlorid-Oxidoarsenate(III) mit der Zusammensetzung $SE_5Cl_3[AsO_3]_4$ (SE = La–Nd, Sm). *Z. Naturforsch.* **2019**, *74b*, 497–506. [CrossRef]
6. Locke, R.J.C. Synthese und Charakterisierung von Seltenerdmetall-Oxidoantimonat(III)-Halogeniden mit Ausläufern zu den entsprechenden Arsenaten und Bismutaten. Ph.D. Thesis, University of Stuttgart, Stuttgart, Germany, 2024. *in preparation*.
7. Gukalova, A.G.; Tseitlin, M.N. Crystal structure of lanthanum fluoroantimonite, $La_5Sb_4O_{12}F_3$. *Kristallografiya* **1988**, *33*, 499–501.
8. Milne, C.J.; Lightfoot, P.; Jorgensen, J.D.; Short, S. Synthesis and Structure of Bi_2LaO_4Cl: A Novel Variant of the Sillén Phases. *J. Matter. Chem.* **1995**, *5*, 1419–1421. [CrossRef]
9. Schmidt, M.; Oppermann, H. Synthese und Kristallstruktur von Bi_2ErO_4I. *Z. Anorg. Allg. Chem.* **1999**, *625*, 544–546. [CrossRef]
10. Schmidt, M.; Oppermann, H.; Henning, C.; Henn, R.W.; Gmelin, E.; Söger, N. Untersuchungen zu Bismutseltenerdoxidhalogeniden der Zusammensetzung Bi_2SEO_4X (X = Cl, Br, I). *Z. Anorg. Allg. Chem.* **2000**, *626*, 125–135. [CrossRef]
11. Kurz, M.V.; Locke, R.J.C.; Erden, A.; Schleid, T. $SmBi_2O_4Cl$: The First Single-Crystal Study in the System $LnBi_2O_4X$. *Acta Crystallogr.* **2022**, *A78*, e528–e529. [CrossRef]
12. Locke, R.J.C.; Schleid, T. The True Nature of $SmSb_2O_4Cl$: Synthesis and Crystal Structure of $Sm_2[Sb_4O_8]Cl_2$ and $Eu_2[Sb_4O_8]Cl_2$. *Z. Anorg. Allg. Chem.* **2022**, *648*, e202200118.
13. Locke, R.J.C.; Goerigk, F.C.; Schäfer, M.J.; Höppe, H.A.; Schleid, T. Synthesis, crystal structures and spectroscopic properties of pure YSb_2O_4Br and YSb_2O_4Cl as well as Eu^{3+}- and Tb^{3+}-doped samples. *Roy. Soc. Chem. Adv.* **2022**, *12*, 640–647. [CrossRef]
14. Locke, R.J.C.; Goerigk, F.C.; Schleid, T. Die Reihe der nicht-zentrosymmetrischen tetragonalen Lanthanoid(III)-Oxidoantimonat(III)-Chloride $LnSb_2O_4Cl$ (Ln = Gd–Lu). *Z. Naturforsch.* **2022**, *77b*, 495–504. [CrossRef]
15. Goerigk, F.C.; Paterlini, V.; Dorn, K.V.; Mudring, A.-V.; Schleid, T. Synthesis and Crystal Structure of the Short $LnSb_2O_4Br$ Series (Ln = Eu–Tb) and Luminescence Properties of Eu^{3+}-Doped Samples. *Crystals* **2020**, *10*, 1089. [CrossRef]
16. Locke, R.J.C.; Goerigk, F.C.; Schleid, T. Unconnected Bromide Layers in the Crystal Structure of $DySb_2O_4Br$. *Z. Kristallogr.* **2021**, *S41*, 78–79.
17. Felsche, J. *Structure and Bonding*; Dunitz, J.D., Hemmerich, P., Ibers, J.A., Jorgensen, C.K., Neilands, J.B., Nyholm, S.R.S., Reinen, D., Williams, R.J.P., Eds.; Springer: Berlin/Heidelberg, Germany; New York, NY, USA, 1973; Volume 13, p. 100.
18. Herrendorf, W.; Bärnighausen, H. *HABITUS: Program for the Optimization of the Crystal Shape for Numerical Absorption Correction in X-SHAPE*; Version 1.06; Stoe & Cie: Darmstadt, Germany, 1999.
19. Sheldrick, G.M. *SHELXS-97 and SHELXL-97: Programs for Solution and Refinement of Crystal Structures from X-ray Diffraction Data*; University of Göttingen: Göttingen, Germany, 1997.
20. Locke, R.J.C.; Bozenhardt, K.-N.; Schleid, T. $Rb_2I_8Nd_4Sb_{16.667}O_{28}$: A Quinary Oxoantimonate(III) Iodide with Rubidium and Neodymium. *Acta Crystallogr.* **2022**, *A78*, e555–e556. [CrossRef]
21. Bozenhardt, K.-N. Synthese und Charakterisierung von Seltenerdmetall(III)-Oxidoantimonat(III)-Iodiden. Master's Thesis, University of Stuttgart, Stuttgart, Germany, 2022.
22. Köhler, W.; Wollan, E. Neutron-diffraction study of the structure of the *A*-form of the rare earth sesquioxides. *Acta Crystallogr.* **1953**, *6*, 741–742. [CrossRef]
23. Brixner, L.H.; Moore, E.P. Single-crystal refinement of the structure of $LaOCl$. *Acta Crystallogr.* **1983**, *C39*, 1316. [CrossRef]
24. Morosin, B. Crystal Structures of Anhydrous Rare-Earth Chlorides. *J. Chem. Phys.* **1968**, *49*, 3007–3012. [CrossRef]
25. Goerigk, F.C.; Schander, S.; Wickleder, M.S.; Schleid, T. The Triclinic Lanthanoid(III) Halide Oxidoarsenates(III) $Sm_3Cl_2[As_2O_5][AsO_3]$ and $Tm_3Br_2[As_2O_5][AsO_3]$. *Z. Anorg. Allg. Chem.* **2020**, *646*, 985–991. [CrossRef]
26. Svenson, C. Refinement of the Crystal Structure of Cubic Antimony Trioxide, Sb_2O_3. *Acta Crystallogr.* **1975**, *B31*, 2016–2018. [CrossRef]
27. Svenson, C. The Crystal Structure of Orthorhombic Antimony Trioxide, Sb_2O_3. *Acta Crystallogr.* **1974**, *B30*, 458–461. [CrossRef]

28. Spek, A.L. *PLATON: A Multipurpose Crystallographic Tool*; Utrecht University: Utrecht, The Netherlands, 2008.
29. Weidlein, J.; Müller, U.; Dehnicke, K. *Schwingungsfrequenzen I—Hauptgruppenelemente*; 1. Auflage, Georg-Thieme-Verlag: Stuttgart, Germany, 1981.
30. Weidlein, J.; Müller, U.; Dehnicke, K. *Schwingungsfrequenzen II—Nebengruppenelemente*; 1. Auflage, Georg-Thieme-Verlag: Stuttgart, Germany, 1986.
31. Häuseler, H.; Jung, M. Single Crystal Grwoth and Structure of LaOBr and SmOBr. *Mater. Res. Bull.* **1986**, *21*, 1291–1294. [CrossRef]
32. Sillen, L.G.; Nylander, A.L. The Crystal Sturcture of LaOCl, LaOBr and LaOI. *Svensk Kem. Tidskr.* **1941**, *53*, 367–372.
33. Lissner, F.; Schleid, T. $Sb_8O_{11}Br_2$: Ein sauerstoffreiches Antimon(III)-Oxidbromid. *Z. Kristallogr.* **2001**, *S18*, 157.
34. Mayerova, Z.; Johnson, M.; Lidin, S. The structure of onoratoite, $Sb_8O_{11}X_2$ (X = Cl, Br) revisited. *Solid State Sci.* **2006**, *8*, 849–854. [CrossRef]
35. Lidin, S.; Johnsson, M.; Hugonin, Z. Modulations in the onoratoite system. *Solid State Sci.* **2009**, *11*, 1198–1205. [CrossRef]
36. Krämer, V. The Crystal Structure of Ferroelastic Antimony(III) Oxide Iodide α-Sb_5O_7I. *Acta Crystallogr.* **1975**, *A31*, 234–237. [CrossRef]
37. Krämer, V. The crystal structure of the ferroelastic/ferroelectric 2*MA* polytype of antimony(III) oxide iodide, Sb_5O_7I. *Acta Crystallogr.* **1978**, *B34*, 2695–2698. [CrossRef]
38. Altenburger, W.; Hiller, W.; Jahn, I.R. Crystal structure of the high-temperature phase of antimony(III) oxide iodide, polytype 2*HA*-Sb_5O_7I. *Z. Kristallogr.* **1987**, *181*, 227–234. [CrossRef]
39. Hugonin, Z.; Johnsson, M.; Lidin, S. Two for the price of one—Resolvable polymorphism in a 'single crystal' of alpha- and beta-Sb_3O_4I. *Solid State Sci.* **2009**, *11*, 24–28. [CrossRef]